PAPER

A rolling circle amplification signal-enhanced immunosensor for ultrasensitive microcystin-LR detection based on a magnetic graphene-functionalized electrode

Zuyu He, Jie Wei, Cuifen Gan, Weipeng Liu* and Yingju Liu [iD]*

A novel competitive immunosensor for the sensitive and selective detection of MC-LR was developed. Magnetic graphene was synthesized, characterized and used as the substrate to immobilize antigens onto the electrode surface due to its surface area and easy separation. Furthermore, gold nanorods were modified with polydopamine and then functionalized with a secondary-antibody and circularization DNA template. By using rolling circle amplification, the DNA template can be replicated to generate extensive repeated DNA sequences, and then hybridized with the detection probe, and thus the signal was remarkably improved. Under the optimal conditions, the proposed immunosensor showed a good linear relationship between the current response and the concentration of MC-LR in the range of 0.01–50 µg L^{-1} with a detection limit of 0.007 µg L^{-1}. The immunosensor was proved to be specific, reproducible and stable. Most importantly, the proposed biosensor was applied to detect MC-LR in a real water sample with good recovery, indicating its potential application in environmental monitoring.

1 Introduction

Cyanotoxins, produced by cyanobacteria or blue-green algae in eutrophic water, are harmful to the health of people and animals across the globe.[1] Microcystins (MCs), one of the most common and hazardous cyanotoxins, have been identified to comprise more than 90 structural variants.[2] Exposure to water contaminated with MCs can result in severe hepatic injury, since MCs can damage the liver by inhibiting the activity of protein phosphatases 1 and 2A.[3] Among all MCs, microcystin-leucine-arginine (MC-LR) is the most widespread and toxic. The World Health Organization (WHO) recommends that the limit of MC-LR should be less than 1 µg L^{-1} in drinking water.[4] Up to now, many analytical techniques have been developed to detect MC-LR, such as high-performance liquid chromatography (HPLC),[5] enzyme-linked immunosorbent assays (ELISA),[6] mass spectrometry[7] and protein phosphatase inhibition assays.[8] However, these methods always need expensive instruments, skilled technicians and complex pre-treatment. Therefore, it is still in need to find precise and sensitive method for qualitative and quantitative determination of MC-LR.

For the last decades, various immunoassay techniques have been developed to detect virus,[9] protein,[10] nucleic acid,[11] heavy metal ions[12] and other small molecules[13] due to their intrinsic characteristics, such as sensitive, selective, time-saving and low-cost. The prerequisite of an electrochemical immunosensor is based on the immobilization of the recognition elements such as antigen or antibody onto the electrode surface. Therefore, appropriate nanomaterials to modify electrode surface can improve the sensitivity and lower the detection limit of an electrochemical immunosensor. Recently, Fe_3O_4 nanoparticles have been applied in toxin-removal,[14] food analysis[15] and biosensor,[16] since they have the abilities of excellent electrical conductivity, biocompatibility and large surface-to-volume ratio. However, raw Fe_3O_4 nanoparticles are lack of active functional groups upon their surfaces, thus it is important to modify them with versatile materials to couple antigen, antibody or other compounds.

In recent years, the two-dimensional carbon nanomaterial graphene becomes the star in nanomaterial family due to its exceptional high surface area, surface functionalization, biocompatibility and high electrical conductivity.[17] Graphene, graphene oxide (GO), reduced graphene oxide (RGO) and their composites have been investigated in many fields, especially in biosensors.[18] The materials that combined GO or RGO with Fe_3O_4 exhibit excellent properties,[19] thus their application in electrode-modified materials is promising and worthy to be exploited. But it should be noted that the direct assembly of Fe_3O_4 on graphene is still a challenge. Polydopamine (PDA), a natural glue formed by spontaneous self-polymerization of dopamine in the presence of oxygen under alkaline condition,

Department of Applied Chemistry, College of Materials & Energy, South China Agricultural University, Guangzhou 510642, China. E-mail: weipeng_liu@scau.edu.cn; liuyingju@hotmail.com; Fax: +86-20-85282366; Tel: +86-20-85280319

has aroused much interest.[20] In addition, its prominent adhesive property makes its easy adherence to almost all types of inorganic or organic substrates. Herein, Fe_3O_4 was treated with dopamine to form Fe_3O_4@PDA, and then magnetic graphene was synthesized by using the hydrothermal treatment of Fe_3O_4@PDA with GO. Especially, during the self-polymerization process of dopamine, catechol groups were oxidized as *ortho*-quinones that provided versatile platform to react with thiol- and amino-groups of antigens *via* Michael addition or Schiff base reaction.[21]

In addition, another significant influence for the sensitivity of the immunosensor is the amount of signal tags onto the sensor surface. Numerous techniques have been explored to amplify the detection signal. For instance, polymerase chain reaction (PCR) is the most widely used technique that has been applied to detect DNA or RNA[22,23] due to its rapid amplification. However, PCR needs expensive instrument, thermal cycling process and rigorous thermostable DNA polymerases.[24] In contrast, rolling circle amplification (RCA), an isothermal DNA amplification technique,[25] can also extend the amount of DNA by generating tens of thousands of repetitive sequences under mild condition. Moreover, the generated repetitive sequences by RCA can hybrid with complementary labelled detection probe DNA to enhance signal response.[26]

In this work, magnetic graphene was synthesized by using the hydrothermal treatment of Fe_3O_4@PDA with GO to immobilize antigens. Then, gold nanorods (AuNR) were utilized to immobilize secondary-antibody and circularization DNA template as the signal label. Rolling circle amplification strategy was carried out to generate massive repeated DNA sequences, and then hybridized with the detection probe, thus the signal of the immunosensor was greatly enhanced. The constructed dual signal amplification immunosensor can be employed to detect MC-LR in real water sample.

2 Experimental

2.1 Materials and apparatus

The antigen (Ag) and the antibody (primary antibody, Ab_1) of MC-LR were gifts from the Guangdong Provincial Key Laboratory of Food Quality and Safety. HRP-labelled goat anti-rabbit secondary antibody (Ab_2) was purchased from Santa Cruz. MC-LR and its related interferences were bought from Enzo Life Sciences Company. Gold(III) chloride tetrahydrate (AuCl$_3$·HCl·4H$_2$O, 99.9%), silver nitrate, sodium dodecyl sulphate (SDS) and hexadecyltrimethyl ammonium bromide (CTAB) were purchased from Shanghai Chemical Reagent Co. Ltd. Dopamine hydrochloride ($C_8H_{11}NO_2$·HCl) were bought from Aladdin Chemistry Co. Ltd. T4 DNA ligase and phi29 DNA polymerase were purchased from Thermo Fisher scientific company. Streptavidin-HRP (ST-HRP), deoxyribonucleoside-5′-triphosphates (dNTP) and the following oligonucleotide sequences were obtained from Shanghai Sangon Biological Engineering Technology & Services Co. Ltd. (China).

Thiolated primer, 5′-SH-(CH$_2$)$_6$-AAA AAA AAA AAA AAA CAC AGC TGA GGA TAG GAC AT-3′;

Circular template, 5′-CTC AGC TGT GTA ACA ACA TGA AGA TTG TAG GTC AGA ACT CAC CTG TTA GAA ACT GTG AAG ATC GCT TAT TAT GTC CTA TC-3′;

Biotinylated DNA probe, 5′-biotin-TTT TTT TCA GAA CTC ACC TGT TAG-3′.

The solution of 0.01 M phosphate buffer saline (PBS, pH = 7.4) contains 0.1370 M of NaCl, 0.0027 M of KCl, 0.0100 M of KH$_2$PO$_4$ and Na$_2$HPO$_4$, while PBST (pH 7.4) was prepared by adding 0.05% Tween 20 into PBS (v/v). 5% skim milk was diluted in 0.01 M PBS as the blocking reagent. The solution of 1/15 M PBS contains 0.1370 M of NaCl, 0.0027 M of KCl, 1/15 M of KH$_2$PO$_4$ and Na$_2$HPO$_4$. All the aqueous solutions were prepared in Milli-Q water.

The morphologies of materials were characterized by transmission electron microscope (TEM, Tecnai 12, FEI, Holland), while the UV-vis and FT-IR spectra were characterized by UV2550 Spectrometer (Shimadzu, Japan) and FT-IR Spectrometer (Nicolet Avatar 360, Thermo, America), respectively. A gel electrophoresis was performed on DYY-6D electrophoresis apparatus (Beijing LiuYi Instrument Company, China). All electrochemical measurements were performed by CHI 660E working station (Shanghai Chenhua Instruments, China) by using indium tin oxide (ITO) electrode as working electrode, Ag/AgCl electrode as reference electrode and the platinum wire as auxiliary electrode, respectively.

2.2 Preparation of Fe_3O_4@PDA/RGO composite

The spherical Fe_3O_4 nanoclusters were synthesized *via* solvothermal method,[27] while graphene oxide was synthesized by modified Hummer's method.[28] To prepare core/shell Fe_3O_4@PDA composites, as shown in Scheme 1B, 10 mg of spherical Fe_3O_4 nanoclusters were dispersed in a mixture of 25 mL of water and 10 mL of ethanol under ultrasonication. An hour later, 15 mL of Tris-8.5 (pH = 8.5) solution was added and sonicated for 30 min, and then 16 mg of dopamine hydrochloride was added and stirred for 18 h under room temperature. The resultant was collected with a magnet, washed and redispersed in 10 mL deionized water. To synthesize Fe_3O_4@PDA/RGO nanocomposites, 5 mg of graphene oxide was dispersed in 20 mL of deionized water, and then mixed with the obtained Fe_3O_4@PDA solution. The mixture was sonicated for one hour, transferred into an autoclave and heated at 130 °C for 8 h. The product was collected with a magnet, washed and redispersed in 3 mL deionized water.

2.3 Synthesis of AuNR@PDA

AuNR was synthesized as following.[29] Firstly, the seed solution was prepared by mixing 5 mL of 0.2 M CTAB solution with 5 mL of 0.5 M HAuCl$_4$ solution in a colorimetric tube, and then 0.6 mL of 10 mM fresh NaBH$_4$ solution was injected and shaken vigorously for one minute. After the colour was changed from yellow to brown, the seed solution was aged at 30 °C under water bath for at least two hours before use.

Secondly, the growth solution was prepared by dissolving 0.7 g of CTAB and 0.1234 g of sodium oleate in 25 mL of deionized water in an Erlenmeyer flask under ultrasonication,
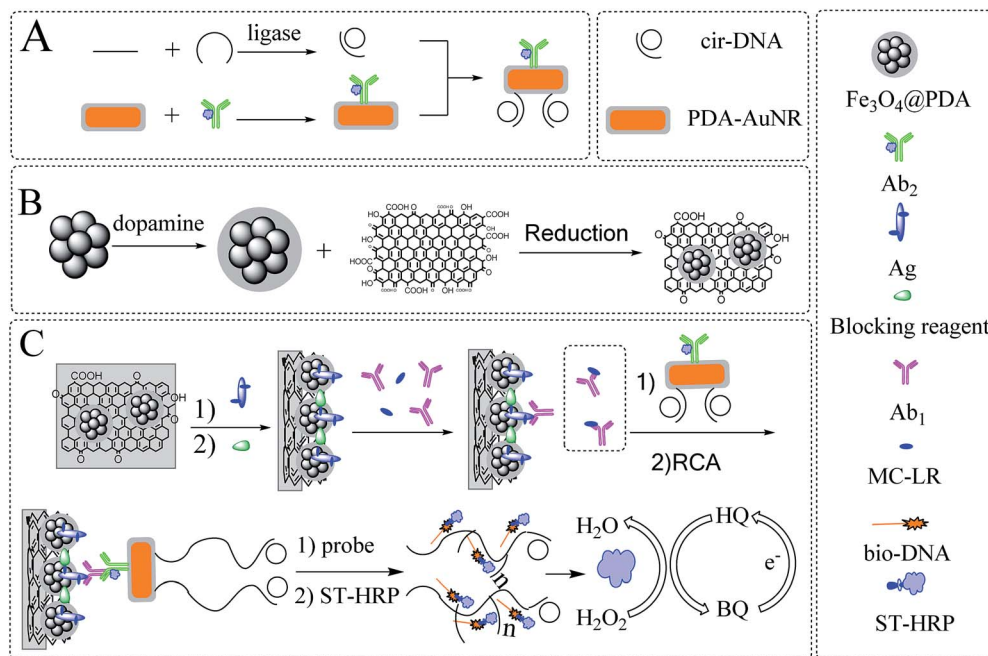
Scheme 1 Illustration of (A) the preparation of Ab$_2$–AuNR–cirDNA, (B) the formation of magnetic graphene composite and (C) the construction process of the proposed MC-LR immunosensor.

and 1.5 mL of 4 mM AgNO$_3$ was added and stirred for 15 min. Then, 25 mL of 1 mM HAuCl$_4$ solution was added and stirred continuously, and the colour of the growth solution was changed from yellow to colorless after adding 0.15 mL of concentrated hydrochloric acid, followed by adding 0.35 mL of 0.0788 M ascorbic acid and stirring for 1 min.

Finally, 60 μL of seed solution was added into the growth solution. The mixture was kept stirring for one minute and aged at 30 °C overnight. After centrifugation and washing, the product was redispersed in 20 mL water as AuNR stock solution. Then, 0.5 mL of AuNR solution was mixed with 5 mL of 0.5 mM dopamine hydrochloride. The solution was sonicated for one hour and centrifuged at 8000 rpm for 10 min to remove the supernatant. After washing, the AuNR@PDA was resuspended in a mixture with 0.5 mL of Tris-8.5 and 0.5 mL of 0.01 M PBST.

2.4 Preparation of Ab$_2$–AuNR–cirDNA conjugate

The circularization DNA template (cirDNA) was prepared as follows.[26] Primer oligonucleotide (1 μM) and template oligonucleotide (1 μM) were mixed in 100 μL of ligation buffer solution (40 mM, Tris–HCl, 10 mM MgCl$_2$, 10 mM DTT (dithiothreitol), 0.5 mM ATP (adenosine triphosphate), and incubated at 37 °C for 1 h). Subsequently, 10 Weiss units of T4 DNA ligase was added and incubated at 37 °C for another 1 h. After ligation, T4 DNA ligase was inactivated by heating at 65 °C for 10 min. The obtained cirDNA mixture could be directly used or stored at −20 °C. To prepare Ab$_2$–AuNR–cirDNA conjugate, as shown in Scheme 1A, 10 μL of Ab$_2$ was mixed with 1 mL of AuNR@PDA solution and stirred at 4 °C for one hour. Subsequently, 100 μL of cirDNA solution was added and stirred

overnight. The Ab$_2$–AuNR–cirDNA resultant was obtained through centrifugation and redispersed in 1 mL of 0.01 M PBST.

2.5 Fabrication of the immunosensor

The fabrication process of the immunosensor was described in Scheme 1C. The working area of the ITO electrode was restricted as 0.4 cm × 0.4 cm by epoxy resin, and washed under sonication by diluted nitric acid (1 : 1), ethanol and deionized water, respectively. Then, 10 μL of 1 mg mL^{-1} fresh dopamine-Tris solution (pH = 8.5) was dropped onto the working area, incubated at 37 °C for 30 min to form thin PDA membrane, and followed by adding 10 μL of diluted Fe$_3$O$_4$@PDA/RGO composites solution (with ethanol, v/v = 9 : 1) onto the sensor surface. After that, 10 μL of MC-LR antigen solution was poured onto the working area, and incubated at 37 °C for 1 h, followed by adding 10 μL of 5% skim milk to block the nonspecific binding sites. The competitive immunoreaction was performed by mixing certain volumes of Ab$_1$ with different known concentrations of MC-LR (dissolved in methanol and diluted in 0.01 M PBS) stock solution, and then incubating with 10 μL of Ab$_2$–AuNR–cirDNA solution for another 1 h.

The rolling circle amplification was initiated by the addition of 10 μL of RCA reaction buffer (33 mM Tris-acetate, pH = 7.9, 10 mM Mg-acetate, 66 mM K-acetate, 0.1% (v/v) Tween 20, 1 mM DTT, 1 unit of phi29 DNA polymerase). After incubating for 1 h at 37 °C, 10 μL of 0.5 μM biotinylated DNA probe was poured onto the electrode and hybridized at 37 °C for 1 h, followed with 10 μL of 20 μg mL^{-1} ST-HRP at 37 °C for 1 h. The electrochemical behaviour of the immunosensor was performed by recording cyclic voltammogram (CV) before and after the addition of 2 mM H$_2$O$_2$ into 10 mL of 1/15 M PBS solution (pH =

7.4) containing 1 mM hydroquinone in the range from -1.0 V to 0.8 V at a scanning rate of 100 mV s^{-1}.

3 Results and discussion

3.1 Characterization of the Fe$_3$O$_4$@PDA/RGO composite

In Fig. 1A, the diameter of the spherical monodispersed magnetic Fe$_3$O$_4$ nanoclusters was about 130 ± 10 nm. After reacting with dopamine, a 10 nm thick PDA layer was generated *via* self-polymerization process to form core/shell structure (Fig. 1B). The as-prepared Fe$_3$O$_4$@PDA composites further reacted with graphene oxide *via* hydrothermal method. Herein, dopamine can be served as a mild and green reductant to reduce GO,[20] but also its aromatic ring and GO provided strong π–π stacking interaction that it was easy for GO to stick onto the surface of PDA.[30] As in Fig. 1C, Fe$_3$O$_4$@PDA was successfully anchored on wrinkle-like RGO.

The FT-IR spectroscopy was further performed to characterize the composite. As seen in Fig. 1D, curve b was for Fe$_3$O$_4$, where the wavenumber of 576 cm^{-1} was corresponded to the Fe–O vibration. After the formation of PDA layer upon Fe$_3$O$_4$ (curve c), two new peaks at 1294 cm^{-1} and 1510 cm^{-1} were found and the peak near 1600 cm^{-1} moved to 1617 cm^{-1}, which were assigned to the phenolic C–OH stretching vibration, the amino N–H shearing and aromatic ring vibration,[31] respectively. As for the Fe$_3$O$_4$@PDA/RGO composite (curve d), the characteristic peak at 3410 cm^{-1} for O–H stretching vibration of GO (curve a) was obviously reduced, while the peaks for epoxy vibration of GO (1224 cm^{-1}, curve a) missed, indicating that GO was partly reduced after the hydrothermal reaction with Fe$_3$O$_4$@PDA. The electrical conductivity of Fe$_3$O$_4$@PDA/RGO composite was increased when GO was reduced to RGO.[18] In addition, the as-prepared Fe$_3$O$_4$@PDA/RGO composite was easily separated by a magnet without traditional centrifugation process and its original morphology and characteristics were perfectly reserved. Besides, the C=O stretching vibration (1628 cm^{-1}) corresponding to the *ortho*-quinones of PDA was found,[32] which could become powerful bridges to react with thiol- and amino-groups of antigens *via* Michael addition or Schiff base reaction.[21] Therefore, by using the abundant *ortho*-quinones of PDA, the large surface-to-volume ratio of Fe$_3$O$_4$, and the excellent conductivity of RGO, sufficient MC-LR antigens can be immobilized onto the magnetic graphene modified electrode.

3.2 Characterization of the Ab$_2$–AuNR–cirDNA composite and RCA product

AuNRs were synthesized *via* seed growth method. From the TEM in Fig. 2A, AuNRs were monodispersed with the width of 30 nm and the length of 80 nm. AuNRs have two special optical surface plasmon bands[33] including the transverse plasmon (TP) band due to the light absorption and scattering along the short axis of the rods and the longitudinal plasmon (LP) band corresponding to the light absorption and scattering along the long axis of the rods. The as-prepared AuNRs possessed a TP band at 523 nm and a LP band at 712 nm. However, in this seed-mediated method, CTAB was used as surfactant to cap AuNRs, but it can hinder AuNRs to link with other biomolecules.[33] Dopamine is easy to self-polymerize under basic condition, thus it was used to modify the AuNRs as a biocompatible material. From the TEM in Fig. 2B, the PDA layer on AuNRs was about 4 nm.

As mentioned above, PDA can generate *ortho*-quinones that provide a versatile platform to link with biomolecules.[21] Therefore, PDA-coated AuNRs were used to associate Ab$_2$ and thiol-cirDNA. In the ultraviolet-visible (UV-vis) spectrum
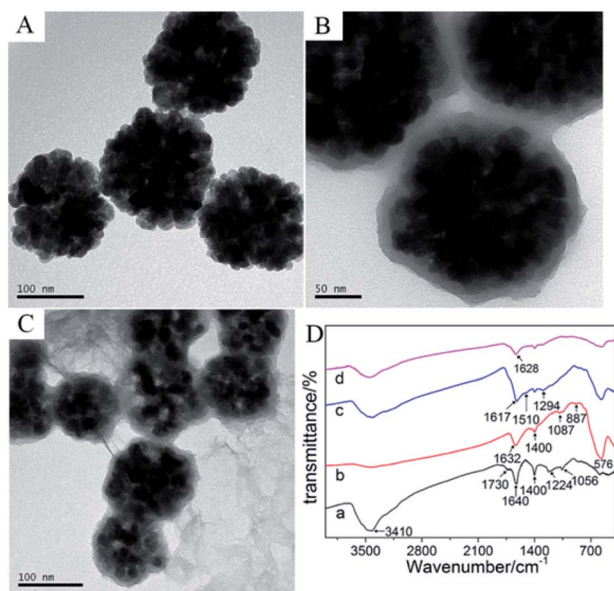

Fig. 1 TEM image of (A) Fe$_3$O$_4$, (B) Fe$_3$O$_4$@PDA, (C) Fe$_3$O$_4$@PDA/RGO, (D) FT-IR spectra of (a) GO, (b) Fe$_3$O$_4$, (c) Fe$_3$O$_4$@PDA and (d) Fe$_3$O$_4$@PDA/RGO.

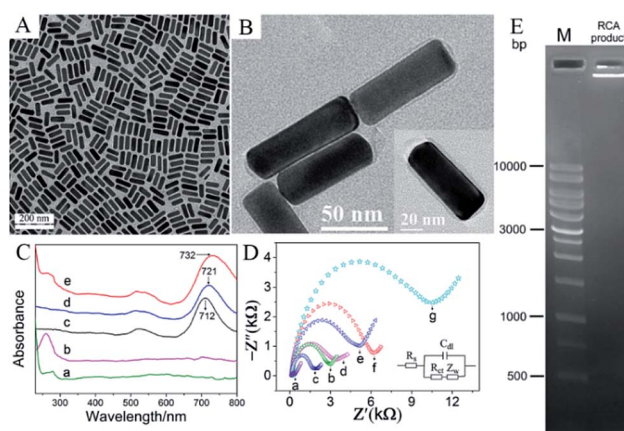**Fig. 2** TEM image of (A) Au NR, (B) AuNR@PDA, (C) UV-vis spectra of (a) Ab$_2$, (b) cirDNA, (c) AuNR, (d) AuNR@PDA and (e) Ab$_2$–AuNR–cirDNA, (D) EIS for (a) bare ITO, (b) PDA/ITO, (c) (Fe$_3$O$_4$@PDA/RGO)/PDA/ITO, (d) Ag/(Fe$_3$O$_4$@PDA/RGO)/PDA/ITO, (e) Ab$_1$/blocking reagent/Ag/(Fe$_3$O$_4$@PDA/RGO)/PDA/ITO, (f) Ab$_2$–AuNR–cirDNA/Ab$_1$/blocking reagent/Ag/(Fe$_3$O$_4$@PDA/RGO)/PDA/ITO, (g) RCA/Ab$_2$–AuNR–cirDNA/Ab$_1$/blocking reagent/Ag/(Fe$_3$O$_4$@PDA/RGO)/PDA/ITO. (E) The image of gel electrophoresis experiment for DNA marker (M) and RCA product.

(Fig. 2C), curve d showed that the LP band of PDA-coated AuNRs was shifted to 721 nm and broader than that of the unmodified AuNRs (curve c). After connecting with Ab_2 and cirDNA, the LP band of AuNRs in curve e was further shifted to 732 nm and became broader. In addition, a broad peak between 280 nm and 260 nm was found, which was corresponded to the overlap of characterized absorption of Ab_2 (curve a) and the typical absorption of cirDNA (curve b), indicating the formation of Ab_2–AuNR–cirDNA conjugate.

The cirDNA conjugated onto AuNRs was further taken to trigger RCA to enhance signal response for the immunoassay. Herein, the agarose gel electrophoretic experiment was performed to verify the rolling circle amplification. The experiment process was as follow. 1% agarose gel was prepared in $0.5\times$ TBE buffer containing 0.01% 4S Green nucleic acid stain and then ran at 120 V for 45 min. From Fig. 2E, compared with the marker lane, the bright lane of RCA product indicated that it was a very long DNA sequence whose structure contained more than 10 000 bp, confirming that rolling circle amplification was carried out.

3.3 Electrochemical study for the fabrication of the immunosensor

The electrochemical impedance spectroscopy (EIS) was used to investigate the assemble process of the immunosensor. It was performed in 5 mM $[Fe(CN)_6]^{3-/4-}$ solution containing 0.1 M KCl, with the frequency ranged from 0.1 Hz to 100 kHz at an amplitude of 50 mV and a bias potential of 0.2 V. The Nyquist plotting of EIS was recorded in Fig. 2D, where the inset is the equivalent circuit model. The R_s, R_{ct}, C_{dl}, and Z_w are the electrolyte solution resistance, the electrode surface charge transfer resistance, the double-layer capacitance and the Warburg impedance, respectively. In the Nyquist plot, a straight line portion at lower frequency range represents the diffusion-limit process. A semicircle section at higher frequency range describes the electrode surface charge transfer resistance (R_{ct}) which corresponds to the electron transfer-limit process. The R_{ct} increases when the surface of electrode prevents the attachment of the redox. From curve a, it showed that the bare ITO electrode owned very small semicircle, indicating its very low electron limit to redox probe. After modifying with PDA, the semicircle (curve b) increased clearly, which meant that the PDA membrane hindered the redox probe to electrode surface. After modification by magnetic graphene composites (curve c), the diameter of semicircle decreased, since RGO possessed good conductivity. When the antigen was immobilized onto the electrode, the R_{ct} increased obviously (curve d), indicating the immobilization of antigens prevented the electron transfer on the electrode. After reacting with Ab_1 (curve e) and Ab_2–AuNR–cirDNA conjugate (curve f), the R_{ct} further increased, suggesting that formation of the immune complex on the electrode surface can retard the electron transfer. After rolling circle amplification, the R_{ct} increased remarkably (curve g) since the negative-charged phosphate backbone of single chain DNA prevented the transfer of $[Fe(CN)_6]^{3-/4-}$ redox probe. All these results confirmed that the fabrication of the immunosensor was accomplished.

3.4 Optimization of the detection conditions for the immunosensor

In order to achieve a sensitive and stable competitive immunosensor, the concentration of Ag, Ab_1, incubation time of Ab_1, and the pH of the detecting system were investigated by using the magnetic graphene composite as substrate and the commercial HRP-labelled Ab_2 as the label. Firstly, the influence of the dilution ratio of antigen was shown in Fig. 3A, where the current response increased quickly when the dilution ratio raised from 1 : 1600 to 1 : 50. The higher dilution ratio of antigen was, the more antigen could be captured onto the electrode. However, the excessive antigen may cause steric hindrance which may lead to the instability for the immunoreaction. On the contrary, the signal response would become very low which could cause high background noise when the immobilized amount of Ag was inadequate. It showed that the current response was very close between the ratio of 1 : 50 and 1 : 100. Therefore, the dilution ratio of 1 : 100 was selected as the optimal concentration of antigen.

Secondly, the dilution ratio of Ab_1 was explored. In Fig. 3B, when the ratio of antibody was diluted from 1 : 100 to 1 : 1600, the current response decreased remarkably, while the dilution ratio of 1 : 100 and 1 : 200 received almost the same signal response, indicating that the 1 : 100 dilution ratio may be oversaturate. The oversaturated concentration of Ab_1 can affect the sensitivity of competitive immunoreaction. So, the 1 : 200 dilution ratio of Ab_1 was chosen.

Subsequently, the reaction time of Ab_1 and Ag was investigated. In Fig. 3C, as the reaction time promoted, the signal response increased. There existed a plateau when the reaction time reached 60 min, or rather, the signal response decreased slowly, when the reaction time was longer. The activity of Ab_1 may weaken when the incubation time was too long. Hence, an hour for incubating was enough.

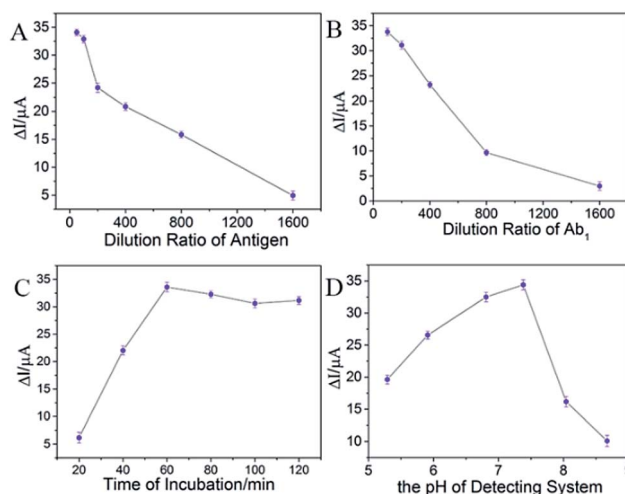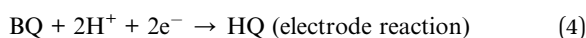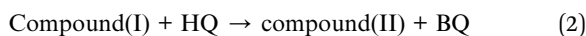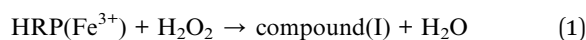Fig. 3 The influence of the conditions on the proposed immunosensor. (A) The dilution ratio of antigen, (B) the dilution ratio of primary antibody, (C) the incubation time of primary antibody and (D) the pH of detecting system.

Finally, the pH of detecting environment was investigated. In Fig. 3D, it showed that when the pH of detecting solution approached neutral, the ideal signal response was recorded. Too much acid or base can decrease the activity of enzyme that resulted in the instability of the immunosensor. Furthermore, the alkaline condition prevented the proton to transfer that the signal response decreased remarkably. So, the optimal pH of 7.38 was chosen.

3.5 The signal enhancement of the immunosensor

The electrochemical behaviour was performed by recording CV before and after the addition of 2 mM of H_2O_2 into 1/15 M PBS solution containing 1 mM hydroquinone. The signal response was recorded from CV through the horseradish peroxidase catalysing the decomposition of hydrogen peroxide. The possible mechanism was described as follows:[16]

$$HRP(Fe^{3+}) + H_2O_2 \rightarrow compound(I) + H_2O \tag{1}$$

$$Compound(I) + HQ \rightarrow compound(II) + BQ \tag{2}$$

$$Compound(II) + HQ \rightarrow HRP(Fe^{3+}) + BQ + H_2O \tag{3}$$

$$BQ + 2H^+ + 2e^- \rightarrow HQ \text{ (electrode reaction)} \tag{4}$$

Herein, the oxidation state and the reduction state of hydroquinone were HQ and BQ, respectively. With the aid of H_2O_2, HRP was oxidized as compound(I). Then HQ reacted with compound(I) to generate BQ. Therefore, as for the electrode reaction, the oxidation peak decreased since HQ was consumed in eqn (2) and (3). On the contrary, the reduction peak increased since a lot of BQ transformed to HQ *via* a two-electron transfer process. In order to estimate the performance of the fabricated immunosensor, three categories of immunosensors were constructed to confirm the signal amplification effect. As shown in Fig. 4A, if PDA was used as the substrate to immobilize antigen and HRP-Ab$_2$ as the label, the current response (ΔI) was 16.32 μA, while if the substrate was replaced by (Fe$_3$O$_4$@PDA/RGO)/PDA, the current response was 33.74 μA. The current response increased substantially that ascribed to two reasons. One reason was that the large surface area of magnetic graphene provided abundant adsorption sites for antigen. The other was that RGO effectively changed the surface electrical conductivity of electrode. Moreover, in Fig. 4C, if Ab$_2$–AuNR–cirDNA was used as the label and the RCA was employed, the current response reached 64.65 μA. RCA can produce repeated units of single chain DNA which can provide plenty of sites for biotinylated DNA probe to hybridize, and then a large number of ST-HRPs were captured by biotinylated DNA probe to improve the signal response. Therefore, magnetic graphene substrate and rolling circle amplification strategy enhanced the signal response of the immunosensor dramatically.

3.6 The performance of the immunosensor

The microcystin-LR analysis was carried out under the optimal condition based on the magnetic graphene substrate using Ab$_2$–AuNR–cirDNA as the label. In a conventional competitive
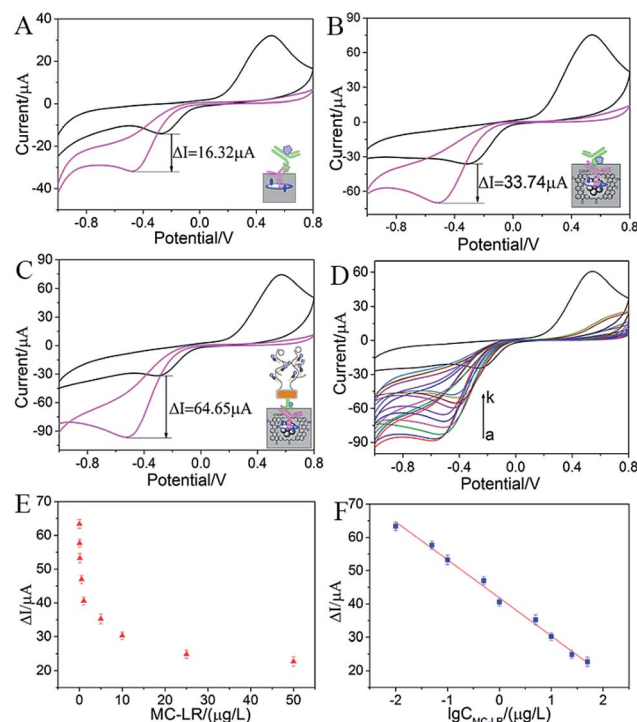

Fig. 4 Different immunosensors of (A) PDA as substrate with HRP-Ab$_2$ label, (B) (Fe$_3$O$_4$@PDA/RGO)/PDA as substrate with HRP-Ab$_2$ label and (C) (Fe$_3$O$_4$@PDA/RGO)/PDA as substrate with Ab$_2$–AuNR–cirDNA label and rolling circle amplification (black lines were CV before while red lines were after the addition of 2 mM H_2O_2 in 1 mM hydroquinone solution). (D) The immunosensor (C) was incubated with different concentrations of MC-LR and then CVs were recorded in 1/15 M PBS solution containing 1 mM hydroquinone after the addition of 2 mM H_2O_2 (from a to j: 0, 0.01, 0.05, 0.1, 0.5, 1, 5, 10, 25 and 50 μg L^{-1}), while curve k was the CV before the addition of H_2O_2. (E) The relationship between the current response (ΔI) and the concentration of MC-LR (C_{MC-LR}). (F) The calibration curve of the proposed immunosensor.

immunosensor, the analyte in the solution can compete with antigen immobilized on the electrode to combine with a certain amount of Ab$_1$. Herein, different concentrations of MC-LR solution were mixed with a certain concentration of Ab$_1$, and a certain volume of mixture was used to incubate with the immobilized antigen. As shown in Fig. 4D, when the concentration of MC-LR increased, the cathodic currents in CVs decreased, suggesting a lower amount of Ab$_1$ was adsorbed on the electrode surface. The current response (ΔI) was denoted as the current change before and after the addition of H_2O_2, showing a clear decrease with the increase in the concentration (Fig. 4E). Especially, the current response showed a linear relationship with the logarithm of MC-LR concentration in the range between 0.01 μg L^{-1} and 50 μg L^{-1} (Fig. 4F). The equation was $\Delta I = 41.82 - 11.44 \times \log C$ ($R^2 = 0.993$), where C was the concentration of MC-LR. According to the equation: $x = 3s/b$, where "s" represents the standard deviation of background signal and "b" is the sensitivity, the detection limit was calculated to be 0.007 μg L^{-1}. The performance of the proposed electrochemical immunosensor was compared with the reported techniques for MC-LR detection. As shown in Table 1, its detection limit and linear range was better than or comparable

Table 1 Comparison of different reported methods for MC-LR detection

Method	Linear range ($\mu g\ L^{-1}$)	LOD ($\mu g\ L^{-1}$)	Ref.
HPLC	—	$0.017\ \mu g\ g^{-1}$	5
ELISA	0.022–0.8	0.022	6
Mass spectrometry	—	0.5	7
Protein phosphatase inhibition	0.93–40.32	0.93	8
Colorimetric inhibition assay	0.098–1.56	0.05	34
Fluorescent aptasensor	0.4–1.2×10^3	0.137	35
Electrochemical impedance aptasensor	4.98×10^{-2} to 1.00×10^2	1.79×10^{-2}	36
Colorimetric sensor	0.5–7.5×10^3	0.37	37
Chemiluminescence enzyme immunoassay	0.062–0.65	0.032	38
Electrochemical immunosensor	0.01–50	0.007	This work

with earlier work. It also met with the need of WHO guideline limit of 1 $\mu g\ L^{-1}$ in drinking water, indicating that it was enough for practical application.

To evaluate the specificity of the immunosensor for the detection of MC-LR, the same amount of MC-LR analogues including MC-RR, MC-YR and nodularin were added into MC-LR and Ab_1 mixture during the incubation process. The "mixture" meant that four microcystins were mixed. Fig. 5 showed that the current response maintained from 94.7% to 97.6%, although the interferences were added, indicating that the proposed immunosensor owned excellent selectivity.

The stability of the proposed immunosensor was investigated. The immunosensor modified by $Ag/(Fe_3O_4@PDA/RGO)/PDA/ITO$ was prepared and put in the refrigerator at 4 °C for two weeks. The current response was still kept 93.75%, indicating that the proposed immunosensor was stable. The repeatability of the immunosensor was evaluated by the coefficients of variation (RSD) of the intra-assay and the inter-assay. The intra-assay precise was investigated by three different concentrations of MC-LR, 0.1 $\mu g\ L^{-1}$, 0.5 $\mu g\ L^{-1}$ and 1 $\mu g\ L^{-1}$ for three parallel experiments, resulting in their RSD of 3.34%, 3.63% and 3.13%, respectively, indicating a good repeatability. The inter-assay precise was estimated by above concentrations of MC-LR in five immunosensors, of whom the coefficients of variation were 3.56%, 3.31% and 3.52%. Therefore, the repeatability of the immunosensor was acceptable.
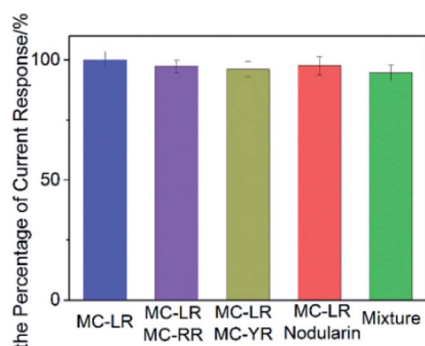

Fig. 5 The specificity of the proposed immunosensor of 1 $\mu g\ L^{-1}$ MC-LR with 1 $\mu g\ L^{-1}$ interferences.

Table 2 Recovery results from the electrochemical immunosensor for MC-LR in lake water

Sample	Added ($\mu g\ L^{-1}$)	Found ($\mu g\ L^{-1}$)	Recovery (%)	RSD (%)
1	1.00	1.05	105.0%	3.13
2	5.00	4.93	98.6%	3.76
3	10.00	9.61	96.1%	2.82

The proposed immunosensor was monitored its practicability by the recoveries of 1 $\mu g\ L^{-1}$, 5 $\mu g\ L^{-1}$ and 10 $\mu g\ L^{-1}$ of MC-LR from the Western Lake water of South China Agricultural University *via* the standard addition method. As shown in Table 2, the recoveries of the spiked sample were 105.0%, 98.6% and 96.1%, respectively. It meant that the proposed immunosensor could be employed in real water sample.

4 Conclusions

In summary, a specific and robust electrochemical immunosensor for MC-LR detection was fabricated based on magnetic graphene substrate and Ab_2–AuNR–cirDNA label. The magnetic graphene composites were used as the substrate to immobilize plenty antigens by taking advantage of their large surface area. Also, the Ab_2–AuNR–cirDNA conjugate was utilized to enhance the current response *via* RCA. Under the optimal conditions, the proposed immunosensor showed excellent performance such as wide linear range from 0.01 $\mu g\ L^{-1}$ to 50 $\mu g\ L^{-1}$ and low detection limit of 0.007 $\mu g\ L^{-1}$. Also, this proposed assembled strategy can be applied to detect MC-LR in real water sample. Therefore, its potential application in environmental monitoring, clinic diagnosis and protein detection can be also expected.

Conflicts of interest

They are no conflicts to declare.

Acknowledgements

Notes and references

1 E. Dittmann and C. Wiegand, *Mol. Nutr. Food Res.*, 2006, **50**, 7–17.
2 S. Singh, A. Srivastava, H. Oh, C. Ahn, G. Choi and R. K. Asthana, *Toxicon*, 2012, **60**, 878–894.
3 M. K. Cordeiro-Araújo, M. A. Chia, J. D. D. T. Arruda-Neto, V. L. Tornisielo, F. Z. Vilca and M. D. C. Bittencourt-Oliveira, *Sci. Total Environ.*, 2016, **566**, 1379–1386.
4 WHO, *Guidelines for drinking-water quality*, World Health Organization, 2004, vol. 1.
5 E. C. Aguete, A. Gago-Martínez, J. M. Leão, J. A. Rodríguez-Vázquez, C. Menàrd and J. F. Lawrence, *Talanta*, 2003, **59**, 697–705.
6 M. Lotierzo, R. Abuknesha, F. Davis and I. E. Tothill, *Environ. Sci. Technol.*, 2012, **46**, 5504–5510.
7 S. Liu, C. Deng and X. Zhang, *Talanta*, 2016, **154**, 183–189.
8 G. Catanante, L. Espin and J. Marty, *Biosens. Bioelectron.*, 2015, **67**, 700–707.
9 R. Xiao, Z. Rong, S. Chen, W. Chen and S. Wang, *RSC Adv.*, 2014, **4**, 36125–36130.
10 Y. Yang, Q. Liu, Y. Liu, Z. Li, Y. Li, P. Wang, D. Zhang, Z. Zhao, Y. Liu and Y. Dong, *RSC Adv.*, 2016, **6**, 31824–31830.
11 H. Yin, B. Sun, Y. Zhou, M. Wang, Z. Xu, Z. Fu and S. Ai, *Biosens. Bioelectron.*, 2014, **51**, 103–108.
12 H. Zhao, C. Xue, T. Nan, G. Tan, Z. Li, Q. X. Li, Q. Zhang and B. Wang, *Anal. Chim. Acta*, 2010, **676**, 81–86.
13 C. Wang, M. Lin, Y. Liu and H. Lei, *Electrochim. Acta*, 2011, **56**, 1988–1994.
14 Y. Deng, D. Qi, C. Deng, X. Zhang and D. Zhao, *J. Am. Chem. Soc.*, 2008, **130**, 28–29.
15 I. S. Ibarra, J. M. Miranda, J. A. Rodriguez, C. Nebot and A. Cepeda, *Food Chem.*, 2014, **157**, 511–517.
16 C. Gan, L. Ling, Z. He, H. Lei and Y. Liu, *Biosens. Bioelectron.*, 2016, **78**, 381–389.
17 Y. Wang, Z. Li, J. Wang, J. Li and Y. Lin, *Trends Biotechnol.*, 2011, **29**, 205–212.
18 C. I. L. Justino, A. R. Gomes, A. C. Freitas, A. C. Duarte and T. A. P. Rocha-Santos, *TrAC, Trends Anal. Chem.*, 2017, **91**, 53–66.
19 V. Georgakilas, J. N. Tiwari, K. C. Kemp, J. A. Perman, A. B. Bourlinos, K. S. Kim and R. Zboril, *Chem. Rev.*, 2016, **116**, 5464–5519.
20 E. K. Jeon, E. Seo, E. Lee, W. Lee, M. Um and B. Kim, *Chem. Commun.*, 2013, **49**, 3392–3394.
21 E. Faure, C. Falentin-Daudré, C. Jérôme, J. Lyskawa, D. Fournier, P. Woisel and C. Detrembleur, *Prog. Polym. Sci.*, 2013, **38**, 236–270.
22 C. Yu, B. Yin, S. Wang, Z. Xu and B. Ye, *Anal. Chem.*, 2014, **86**, 7214–7218.
23 A. McBeath, N. Bain, M. Fourrier, B. Collet and M. Snow, *J. Virol. Methods*, 2013, **187**, 65–71.
24 W. Cheng, F. Yan, L. Ding, H. Ju and Y. Yin, *Anal. Chem.*, 2010, **82**, 3337–3342.
25 M. M. Ali, F. Li, Z. Zhang, K. Zhang, D. Kang, J. A. Ankrum, X. C. Le and W. Zhao, *Chem. Soc. Rev.*, 2014, **43**, 3324–3341.
26 H. Chen, S. Wu, F. Dong, W. Cheng, Q. Li, S. Ding and R. Luo, *Sens. Actuators, B*, 2015, **221**, 328–333.
27 M. Lin, H. Huang, Z. Liu, Y. Liu, J. Ge and Y. Fang, *Langmuir*, 2013, **29**, 15433–15441.
28 C. Gan, Z. Sun, L. Ling, Z. He, H. Lei and Y. Liu, *RSC Adv.*, 2016, **6**, 51662–51669.
29 X. Ye, C. Zheng, J. Chen, Y. Gao and C. B. Murray, *Nano Lett.*, 2013, **13**, 765–771.
30 Y. Yang, A. M. Asiri, Z. Tang, D. Du and Y. Lin, *Mater. Today*, 2013, **16**, 365–373.
31 T. Zeng, X. Zhang, Y. Ma, H. Niu and Y. Cai, *J. Mater. Chem.*, 2012, **22**, 18658–18663.
32 M. Liu, G. Luo, Y. Wang, R. Xu, Y. Wang, W. He, J. Tan, M. Xing and J. Wu, *Sci. Rep.*, 2017, **7**, 436.
33 Z. Zhang and M. Lin, *RSC Adv.*, 2014, **4**, 17760–17767.
34 A. Sassolas, G. Catanante, D. Fournier and J. L. Marty, *Talanta*, 2011, **85**, 2498–2503.
35 S. M. Taghdisi, N. M. Danesh, M. Ramezani, N. Ghows, S. A. M. Shaegh and K. Abnous, *Talanta*, 2017, **166**, 187–192.
36 Z. Lin, H. Huang, Y. Xu, X. Gao, B. Qiu, X. Chen and G. Chen, *Talanta*, 2013, **103**, 371–374.
37 X. Li, R. Cheng, H. Shi, B. Tang, H. Xiao and G. Zhao, *J. Hazard. Mater.*, 2016, **304**, 474–480.
38 F. Long, H. C. Shi, M. He, J. W. Sheng and J. F. Wang, *Anal. Chim. Acta*, 2009, **649**, 123–127.